



## Enhanced sulfur in the UTLS in spring 2020

Laura Tomsche<sup>1,2</sup>, Andreas Marsing<sup>1,2</sup>, Tina Jurkat-Witschas<sup>1</sup>, Johannes Lucke<sup>1,5</sup>, Stefan Kaufmann<sup>1</sup>,  
Katharina Kaiser<sup>3</sup>, Johannes Schneider<sup>3</sup>, Monika Scheibe<sup>1</sup>, Hans Schlager<sup>1</sup>, Lenard Röder<sup>3</sup>, Horst  
5 Fischer<sup>3</sup>, Florian Obersteiner<sup>4</sup>, Andreas Zahn<sup>4</sup>, Jos Lelieveld<sup>3</sup>, Christiane Voigt<sup>1,2</sup>

<sup>1</sup>German Aerospace Center, 82234 Weßling, Germany

<sup>2</sup>Johannes Gutenberg University Mainz, 55099 Mainz, Germany

<sup>3</sup>Max Planck Institute for Chemistry, 55128 Mainz, Germany

<sup>4</sup>Karlsruhe Institute for Technology (KIT), 76021 Karlsruhe, Germany

10 <sup>5</sup>Faculty of Aerospace Engineering, Delft University of Technology, 2629 Delft, Netherlands

*Correspondence to:* Laura Tomsche (ltomsche@uni-mainz.de)

**Abstract.** Sulfur compounds in the upper troposphere and lower stratosphere (UTLS) impact the atmosphere radiation budget, either directly as particles or indirectly as precursor gas for new particle formation. In situ measurements in the UTLS are rare, but are important to better understand the impact of the sulfur budget on climate. The BLUESKY mission in May/June 2020 explored an unprecedented situation. 1) The UTLS experienced extraordinary dry conditions in spring 2020 over Europe, in comparison to previous years and 2) the first lockdown of the COVID-19 pandemic caused major emission reductions from industry, ground, and airborne transportation. With the two research aircraft HALO and Falcon, 20 flights were conducted over Central Europe and the North Atlantic to investigate the atmospheric composition with respect to trace gases, aerosol, and clouds. Here, we focus on measurements of sulfur dioxide (SO<sub>2</sub>) and particulate sulfate (SO<sub>4</sub><sup>2-</sup>) in the altitude range of 8 to 14.5 km which show unexpectedly enhanced mixing ratios of SO<sub>2</sub> in the upper troposphere and of SO<sub>4</sub><sup>2-</sup> in the lowermost stratosphere. In the UT, we find SO<sub>2</sub> mixing ratios of (0.07±0.01) ppb, caused by the remaining air traffic, reduced SO<sub>2</sub> sinks due to low OH and low cloud fractions, and to a minor extent by uplift from boundary layer sources. Particulate sulfate showed elevated mixing ratios of up to 0.33 ppb in the LS. We suggest that the eruption of the volcano Raikoke in June 2019, which emitted about 1 Tg SO<sub>2</sub> into the stratosphere in northern midlatitudes caused these enhancements, in addition to Siberian and Canadian wildfires and other minor volcanic eruptions. Our measurements can help to test models and lead to new insights in the distribution of sulfur compounds in the UTLS, their sources and sinks. Moreover, these results can contribute to improve simulations of the radiation budget in the UTLS with respect to sulfur effects.

15  
20  
25

### 1 Introduction

The stratospheric aerosol layer changes in time, especially after volcanic eruptions with plume injection heights into the stratosphere, the layer gets more pronounced (Kremser et al., 2016). It plays a role in the radiative balance and thus impacts the climate (Solomon et al., 2011). An enhanced aerosol concentration leads to a larger albedo. The geo engineering community

30



investigates the enhancement of the aerosol layer with injections of sulfur compounds into the stratosphere to partly counteract greenhouse gases related global warming (Crutzen, 2006; Schäfer et al., 2015). The stratospheric aerosol layer is often referred to as “Junge layer” and can extend from the tropopause up to 25 km (Junge et al., 1961). The chemical composition of the stratospheric aerosol layer is dominated by sulfate ( $\text{SO}_4^{2-}$ ) particles, which consist mainly of pure sulfuric acid droplets, sulfuric acid with material from ablated meteoroids or mixed organic-sulfate particles (Murphy et al., 2014; Cziczo et al., 2001; Schneider et al., 2021). During volcanic quiescent periods, precursor gases, like carbonyl sulfide (OCS), and non-volcanic sulfur dioxide ( $\text{SO}_2$ ), as well as tropospheric  $\text{SO}_4^{2-}$  particles preserve the stratospheric layer (Brock et al., 1995). Due to its long lifetime, OCS is vertically uplifted from the tropics into the stratosphere and there it converts mostly through photodissociation to  $\text{SO}_2$  (Sheng et al., 2015). The  $\text{SO}_2$  chemistry and transport depends strongly on the ambient conditions. In the free troposphere and lower stratosphere,  $\text{SO}_2$  reacts predominantly with hydroxyl (OH) to sulfuric acid ( $\text{H}_2\text{SO}_4$ ) (English et al., 2011; Stockwell and Calvert, 1983), thus the lifetime correlates with the OH concentration. At cold temperatures and in the presence of water vapour, the gaseous  $\text{H}_2\text{SO}_4$  condenses quickly to particles (Almeida et al., 2013; Kirkby et al., 2011), thereby forming sulfate aerosol. In the boundary layer, pollution could significantly reduce the lifetime to hours (Lee et al., 2011) and consequently, also the transport of  $\text{SO}_2$  to higher altitudes. Clouds could also limit the  $\text{SO}_2$  lifetime to hours or days (Lelieveld et al., 1993), as the conversion of  $\text{SO}_2$  to  $\text{H}_2\text{SO}_4$  is faster in cloud droplets than in the gas phase (Seinfeld and Pandis, 2006). Nevertheless,  $\text{SO}_2$  can be transported from the planetary boundary layer (PBL) into the UTLS region via different pathways. Similar to OCS,  $\text{SO}_2$  can be vertically transported across the tropical tropopause layer (TTL) or by overshooting convection in the tropics (Fueglistaler et al., 2009) or by the transport of  $\text{SO}_2$  in a warm conveyor belt (WCB) in the midlatitudes (Arnold et al., 1997; Clarisse et al., 2011; Fiedler et al., 2009) or by transport processes connected with the Asian monsoon (Gottschaldt et al., 2017, 2018; Ploeger et al., 2017; Tomsche et al., 2019; Vogel et al., 2019; von Hobe et al., 2021). An explosive volcanic eruption can inject huge amounts of ash,  $\text{SO}_2$ , and other volcanic gases into the stratosphere and thus enhance the stratospheric aerosol layer (Kremser et al., 2016). In 1991, the volcano Mount Pinatubo ( $15^\circ\text{N}$ ) emitted approximately 20 Tg of  $\text{SO}_2$  and 30 Tg of aerosol (McCormick et al., 1995), which impacted the stratosphere globally. Volcanic eruptions in midlatitudes can also impact the stratosphere, e.g. Mount St Helens ( $46^\circ\text{N}$ ,  $\text{SO}_2=0.8$  Tg) in 1980, but its impact vanished in about a year (Deshler et al., 2006). One recent midlatitude eruption of similar strength was the volcano Raikoke in June 2019 ( $48.28^\circ\text{N}$ , Kloss et al., 2021, de Leeuw et al., 2021) which emitted approx. 1.4-1.6 Tg  $\text{SO}_2$ . A further important source of stratospheric aerosol are intense wildfires, which can potentially develop pyrocumulonimbus (pyroCb) and thus transport biomass burning emissions into the UTLS (Fromm et al., 2005; Peterson et al., 2018). Moreover, air traffic is another source of particles and precursor gases in the UTLS (Lee et al., 2010; Voigt et al., 2010; Jurkat et al., 2011). In late spring 2020, the UTLS region was probed over Europe during the BLUESKY mission, the period covered the first weeks of the COVID19 lockdown in Europe, which caused reductions in emissions from industry, ground, and especially airborne transportation (Voigt et al., 2022). Under these conditions, we found enhanced values of  $\text{SO}_2$  in the upper troposphere (UT) and of particulate  $\text{SO}_4^{2-}$  in the lowermost stratosphere (LS), which motivated us to investigate these sulfur compounds with respect to their sources and sinks.



In the following, we first present the BLUESKY mission in section 2. In section 3.1, we introduce the airborne measurements and in section 3.2 the trace gas and particulate profiles obtained during BLUESKY and also show tropospheric and stratospheric influenced compounds in tracer-tracer correlations (section 3.3). Afterwards, we focus on the SO<sub>2</sub> profile in the UT (section 4) and continue in section 5 with the stratospheric sulfate aerosol. Finally, we summarize our results and give an outlook in section 6.

## 2 Methods

### 2.1 BLUESKY mission

The BLUESKY mission was led by the German Aerospace Center (DLR) and the Max-Planck-Institute for Chemistry, Mainz. Coordinated flights were performed from Oberpfaffenhofen with the High-Altitude and Long-Range Research Aircraft HALO and the DLR Falcon over Europe and the North Atlantic between 16 May and 09 June 2020. In total 20 flights were performed (Fig. 1). The period covered the first weeks of the COVID-19 lockdown in Europe. Both aircraft were equipped with in situ instruments to investigate trace gases, aerosols, and cloud properties. An overview of the BLUESKY mission is given in Voigt et al. (2022) and further detailed studies are published by Schumann et al. (2021a, 2021b), Reifenberg et al. (2021), Nussbaumer et al. (2021), Hamryszczak et al. (2022) and Krüger et al. (2022). In the present study we will focus on the sulfur compounds in the upper troposphere and lower stratosphere.

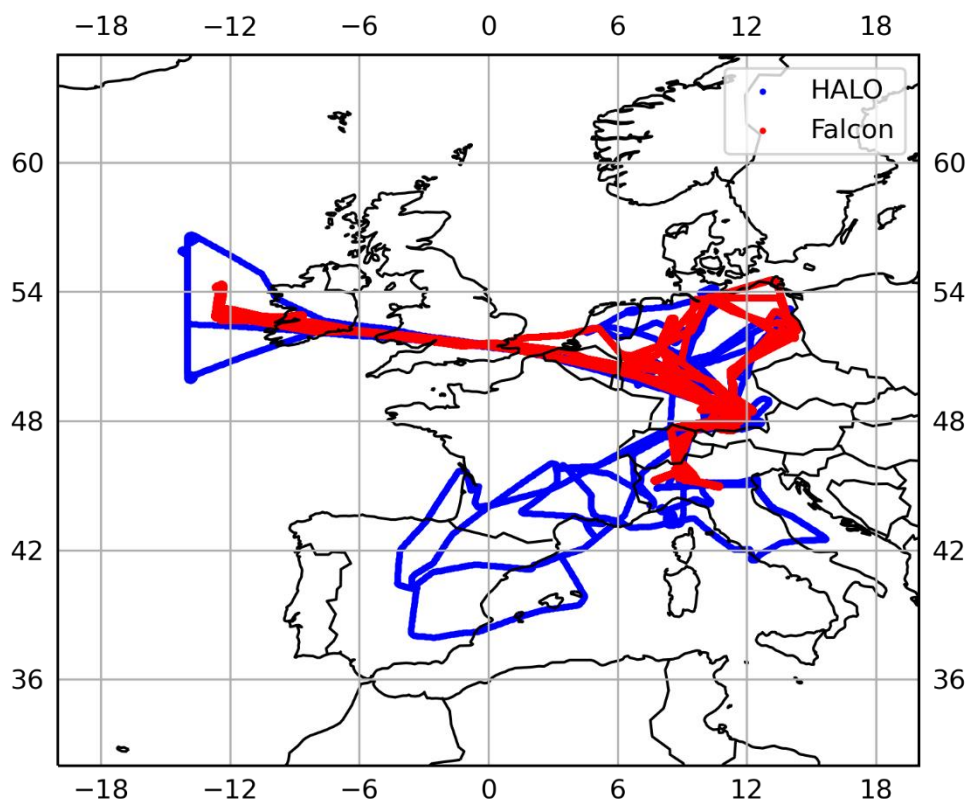


**Figure 1: Overview of all flight tracks performed by Falcon (red) and HALO (blue) during the BLUESKY mission in May/June 2020 during the COVID19 lockdown.**

## 85 2.2 Instrumentation

In the present study several trace gas measurements onboard Falcon and also trace gas and particle measurements onboard HALO are used. Onboard Falcon, the atmospheric chemical ionization mass spectrometer AIMS measures gaseous  $\text{SO}_2$  and nitric acid ( $\text{HNO}_3$ ) among other compounds at mixing ratios relevant for the UTLS region by using  $\text{SF}_5^-$  as reagent ion. A more detailed description of the instrument can be found elsewhere (Voigt et al., 2014; Jurkat et al., 2016; Marsing et al.,  
90 2019).  $\text{SO}_2$  is calibrated in flight using an isotopically labelled calibration gas mixture of the isotope  $^{34}\text{SO}_2$ , which is heavier than the naturally dominant isotope  $^{32}\text{SO}_2$ , but has the same chemical behaviour (Jurkat et al., 2016). The natural isotopic ratio is  $^{34}\text{S}/^{32}\text{S} = 0.0454$  and the mass spectrometer can detect both isotopes separately as they differ in mass by 2 amu (atomic mass units). This has the advantage that the calibration gas can be continuously added to the sampling flow and the system is well conditioned for  $\text{SO}_2$ . A drawback is that the background of the instrument is increased by 5%, due to



95 impurities of  $^{32}\text{SO}_2$  in the calibration gas. The  $\text{SO}_2$  data are instrument background corrected, which includes a moisture  
correction, as higher water vapour concentrations lead to cross sensitivities on  $m/z = 83$  amu ( $\text{FSO}_2^-$ ; Jurkat et al., 2016). With  
increasing moisture in lower altitudes, a correction is more difficult, thus we focus on altitudes above 8 km. The other trace  
gas measured by AIMS is  $\text{HNO}_3$ , which is in-flight calibrated using a permeation oven with a solution of  $\text{HNO}_3$  in water  
(Jurkat et al., 2014). The data are background corrected including a moisture correction, which is necessary to account for  
100 cross sensitivities caused by water vapour (Jurkat et al., 2016). The AIMS measurements were performed with a 1.6 sec time  
resolution and smoothed with a running mean of 20 seconds. The  $1\sigma$  detection limit of  $\text{SO}_2$  varied between 0.006-0.017 ppb.  
The total uncertainty is on average 22.7% for  $\text{SO}_2$ . The  $1\text{-}\sigma$  detection limit for  $\text{HNO}_3$  is in the range of 0.005-0.009 ppb. The  
 $\text{HNO}_3$  total uncertainty is on average 16% (Marsing, 2021). Further measurements onboard Falcon included CO and  $\text{O}_3$ .  $\text{O}_3$   
was measured using a UV photometer (Schulte and Schlager, 1996; Ziereis et al., 2000), CO was measured by cavity ring  
105 down spectroscopy (Klausner et al., 2020). The accuracies for CO and  $\text{O}_3$  are 15% and 5%, respectively.

Onboard HALO, the compact time-of-flight aerosol mass spectrometer (C-ToF-AMS) measured the aerosol composition  
(Drewnick et al., 2005; Schmale et al., 2010; Schulz et al., 2018). Aerosol particles of approximately 50 to 800 nm are analysed,  
which then provides quantitative mass concentrations of organic matter, sulfate, nitrate and ammonium. The instrument is  
equipped with a constant pressure inlet that ensures a steady mass flow and an operation pressure of the aerodynamic lens for  
110 stable inflight operation (Molleker et al., 2020). Here, we focus on sulfate. For a better comparability of  $\text{SO}_4^{2-}$  with  $\text{SO}_2$ , we  
calculate mixing ratios (ppb) instead of using concentrations ( $\mu\text{g m}^{-3}$ ). Additionally, mixing ratios have the advantage of being  
pressure independent. We assumed that all  $\text{SO}_4^{2-}$  would be evaporated and calculated the volumetric mixing ratio for  $\text{SO}_4^{2-}$ .  
Above 8 km, the  $1\sigma$  detection limit is  $(0.006 \pm 0.001)$  ppb for  $\text{SO}_4^{2-}$ , the accuracy is 30% and the precision on average  
 $(0.002 \pm 0.001)$  ppb (Schulz et al., 2018). Additionally, the trace gases CO and  $\text{O}_3$  onboard HALO are considered in the present  
115 study for altitudes above 8 km. CO was measured by the TRacer In-Situ Tdlas for Atmospheric Research (TRISTAR; Schiller  
et al., 2008) with a total uncertainty of 3 % for tropospheric measurements (Nussbaumer et al., 2021). Note that due to a small  
Nitrous oxide ( $\text{N}_2\text{O}$ ) interference the uncertainty in the lower stratosphere is higher ( $8.5 \pm 3.9$  ppbv).  $\text{O}_3$  was measured by the  
Fast Airborne Ozone instrument FAIRO, which combines the technique of a UV photometer and a chemiluminescence detector  
(Zahn et al., 2012). The  $\text{O}_3$  total uncertainty was 2-2.5%.  
120  $\text{SO}_2$  was sampled onboard Falcon and  $\text{SO}_4^{2-}$  was probed onboard HALO. Nevertheless, campaign averaged CO and  $\text{O}_3$  profiles  
from both aircraft agree and motivate the combined interpretation of the  $\text{SO}_2$  and  $\text{SO}_4^{2-}$  distributions during spring 2020 (see  
Sec. 3.2).

### 2.3 Trajectory calculations

Back trajectory calculations were performed using the HYSPLIT atmospheric transport and dispersion model (Stein et al.,  
125 2015; Rolph et al., 2017) with the GDAS (Global Data Assimilation System) meteorological dataset. For selected cases with  
elevated  $\text{SO}_2$  mixing ratios, 360 h back trajectories were calculated for nine starting points. We used three locations

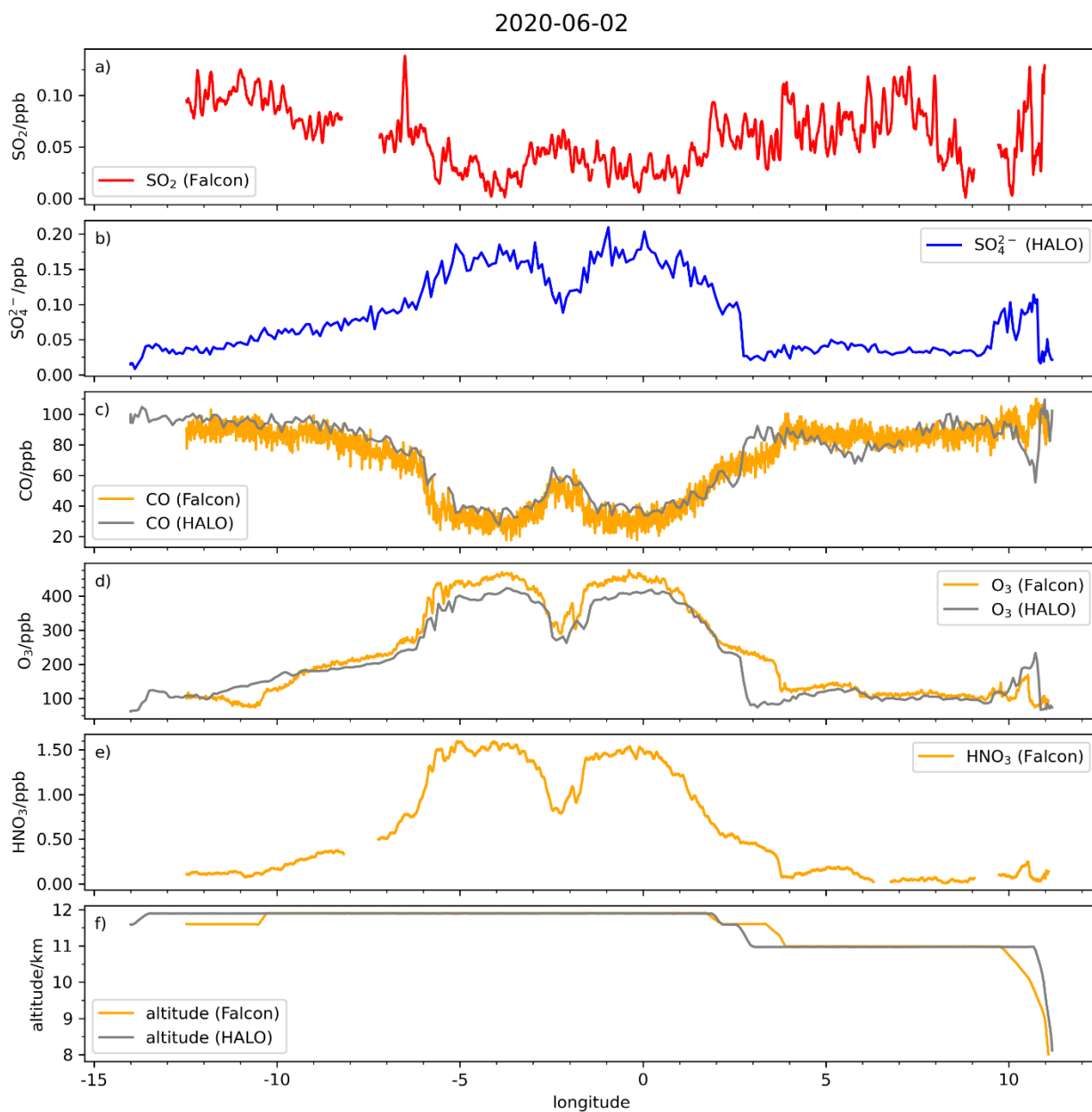


(longitude/latitude) along the flight track, which reflect before, at, and after the event, and for each location, we varied the altitude to 8000, 10000, and 12000 m. With the help of the back trajectories, air mass origins and transport pathways in the atmosphere could be identified.

## 130 3 Results

### 3.1 Trace gases along flight track

On 02 June 2020, HALO and Falcon took off in Oberpfaffenhofen and headed towards the North Atlantic, west of Ireland, with similar flight tracks, altitude and similar take-off time. With a shorter flight range, Falcon landed in Shannon/ Ireland to refuel, while HALO continued its flight. In Figure 2, flight altitude and in situ measurements are plotted against longitude for comparability from both aircraft for the time between 7:00 and 10:00 UTC. O<sub>3</sub> and CO were measured aboard both aircraft. Both trace gases show similar patterns independent of the aircraft. The highest O<sub>3</sub> mixing ratios with maxima of 475 ppb (Falcon) and 423 ppb (HALO) were approximately between 6°W and 3°E, while CO had the lowest mixing ratios of 18 ppb (Falcon) and 28 ppb (HALO) along the same longitudes and vice versa, when CO mixing ratios were enhanced with maxima of 110 ppb (Falcon) and 109 ppb (HALO), O<sub>3</sub> mixing ratios were low (Falcon: 74 ppb, HALO: 62 ppb). Because CO and O<sub>3</sub> from both platforms agree within their uncertainties and reflect the same trends, we assume that both aircraft probed the same air mass. HNO<sub>3</sub> reflects the O<sub>3</sub> behaviour quite well, with enhanced mixing ratios up to 1.6 ppb in the mentioned longitude range. A similar trend can be observed in the particulate compound SO<sub>4</sub><sup>2-</sup>, which also is enhanced when O<sub>3</sub>, as a stratospheric tracer, is enhanced. SO<sub>4</sub><sup>2-</sup> ranges from the detection limit to 0.21 ppb. SO<sub>2</sub> mixing ratios show a larger variability, but in general, they follow the CO mixing ratios, which is a tropospheric tracer (Fischer et al., 2000; Hoor et al., 2002). SO<sub>2</sub> ranges from the detection limit to 0.15 ppb and experiences one short peak with 0.15 ppb around 6.5°W at an altitude of 11.9 km. Other trace gases onboard Falcon measured to 266 ppb O<sub>3</sub>, 70 ppb CO, and 0.8 ppb HNO<sub>3</sub> during this event, but beside HNO<sub>3</sub>, which increased slightly, CO and O<sub>3</sub> showed no perturbations around this location. Back trajectory analysis (Fig. 5i) indicate mostly long-range transport at high altitudes.



150

**Figure 2:** On 02 June 2020, HALO and Falcon had similar flight tracks from Oberpfaffenhofen towards the North Atlantic, west of Ireland. The sampling was roughly between 7-10 UTC. Plotted are in a)  $\text{SO}_2$ , b)  $\text{SO}_4^{2-}$  c) CO, d)  $\text{O}_3$ , e)  $\text{HNO}_3$  and f) altitude.



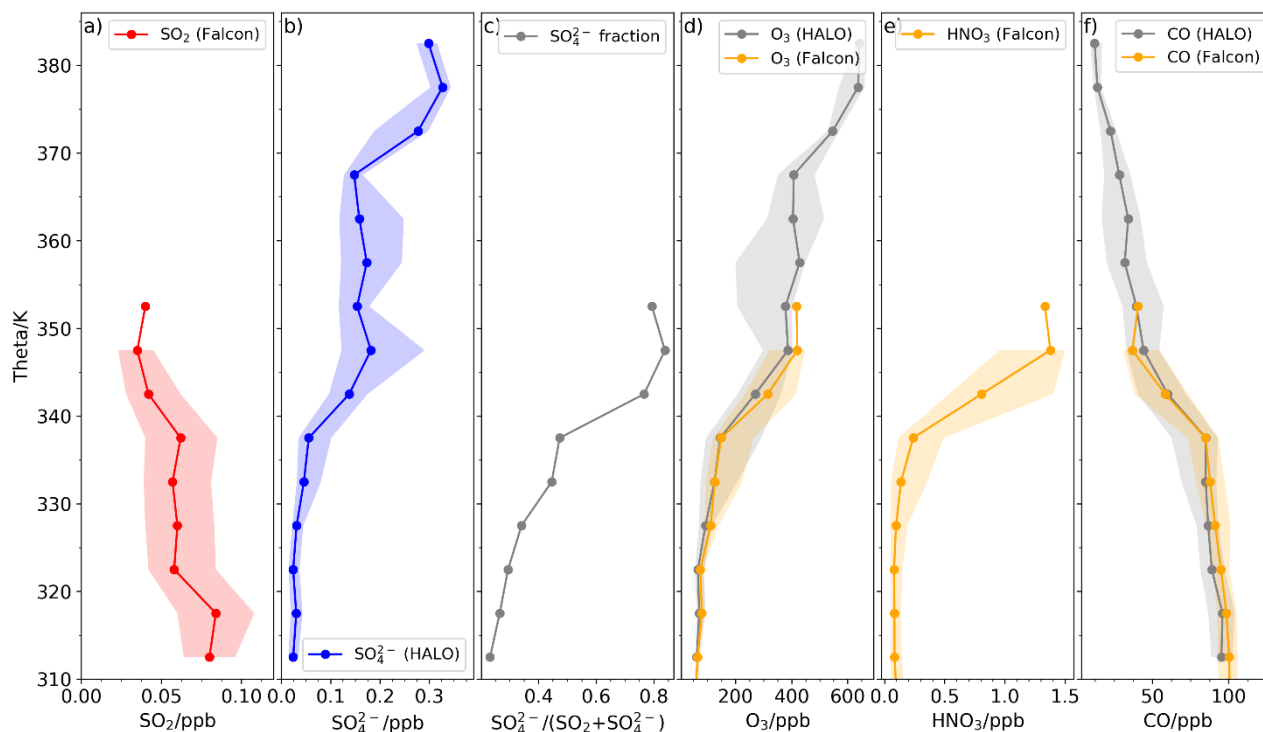
### 3.2 SO<sub>2</sub> and SO<sub>4</sub><sup>2-</sup> median profiles

155 Following the case mentioned above, we broaden our analysis to all flights of the whole campaign. In Figure 3, median, 25<sup>th</sup>  
and 75<sup>th</sup> percentile profiles of the trace gases and the particulate compounds are displayed with the potential temperature as a  
vertical axis. The medians, 25<sup>th</sup> and 75<sup>th</sup> percentiles are calculated for 5 K potential temperature bins from 310 K to 355 K  
for Falcon flights and up to 385 K for HALO flights. The Falcon profile is limited in height due to the maximum flight  
altitude of approx. 12.5 km in comparison to HALO with a ceiling altitude of 14.5 km. First, we compare the trace gases  
160 measured on both aircraft, Falcon and HALO. The stratospheric tracer O<sub>3</sub> behaves similar for both aircraft within the 25<sup>th</sup>  
and 75<sup>th</sup> percentiles with a step around 340 K, while the spread between the percentiles starts to increase already around  
330 K. Below this altitude, median O<sub>3</sub> mixing ratios reach minima of 41 ppb (Falcon) and 62 ppb (HALO) and above they  
rise up to 420 ppb (Falcon) and 642 ppb (HALO). According to Thouret et al. (2006), we use a O<sub>3</sub> threshold of 120 ppb as  
the chemical tropopause, which corresponds here to a potential temperature of 330 K, even though most tracers experience a  
165 stepwise increase around 340 K. The tropospheric tracer CO from both platforms has similar profiles with median mixing  
ratios of 37-112 ppb (Falcon) and 12-96 ppb (HALO). Both CO profiles show a decrease with height, thus anticorrelated to  
O<sub>3</sub>, but they reflect a significant change in the mixing ratios at 340 K, similar to O<sub>3</sub>. Additionally, the median HNO<sub>3</sub> profile  
follows the trend of O<sub>3</sub> with low mixing ratios down to 0.3 ppb followed by a steep increase around 340K and reaches a  
maximum of 1.4 ppb. Between 330 K and 350 K, the stratospheric tracers O<sub>3</sub> and HNO<sub>3</sub>, as well as the tropospheric tracer  
170 CO show larger variations between the percentiles, which indicates the mixing layer described by Hoor et al. (2002) over the  
course of the mission. As shown, the profiles for O<sub>3</sub> and CO for HALO and Falcon flight tracks agree well within their 25<sup>th</sup>  
and 75<sup>th</sup> percentiles. Both aircraft probed the atmosphere above Europe and the North Atlantic within the mission period and  
thus during similar meteorological conditions, even though the days and routes partly differ. This gives us confidence to  
further investigate and compare measurements of sulfur compounds sampled on both aircraft: SO<sub>2</sub> was sampled on Falcon,  
175 while SO<sub>4</sub><sup>2-</sup> was probed on HALO. Profiles of SO<sub>2</sub> and SO<sub>4</sub><sup>2-</sup> are shown in Fig. 3a and 3b, respectively. The median SO<sub>2</sub>  
profile decreases with height and median values range from 0.05 ppb to 0.08 ppb with the lowest mixing ratios above 330 K.  
The opposite behaviour can be observed in the median SO<sub>4</sub><sup>2-</sup> profile, which increases with height. The mixing ratios are  
lowest at 0.02 ppb and raise up to 0.33 ppb. The profile shows a similar trend in comparison to O<sub>3</sub> with a stepwise increase





180 around 340 K. The enhanced  $\text{SO}_4^{2-}$  mixing ratios above the chemical tropopause can be associated with the stratospheric sulfate aerosol.



185 **Figure 3: Median profiles with 25th and 75th percentiles as shaded areas are shown for trace gases with the potential temperature as vertical axes. The data are calculated for 5K potential temperature bins. In: a)  $\text{SO}_2$ , b)  $\text{SO}_4^{2-}$ , c) the  $\text{SO}_4^{2-} / (\text{SO}_2 + \text{SO}_4^{2-})$  ratio d)  $\text{O}_3$ , e)  $\text{HNO}_3$  and f)  $\text{CO}$  for measurements performed on HALO and Falcon.**

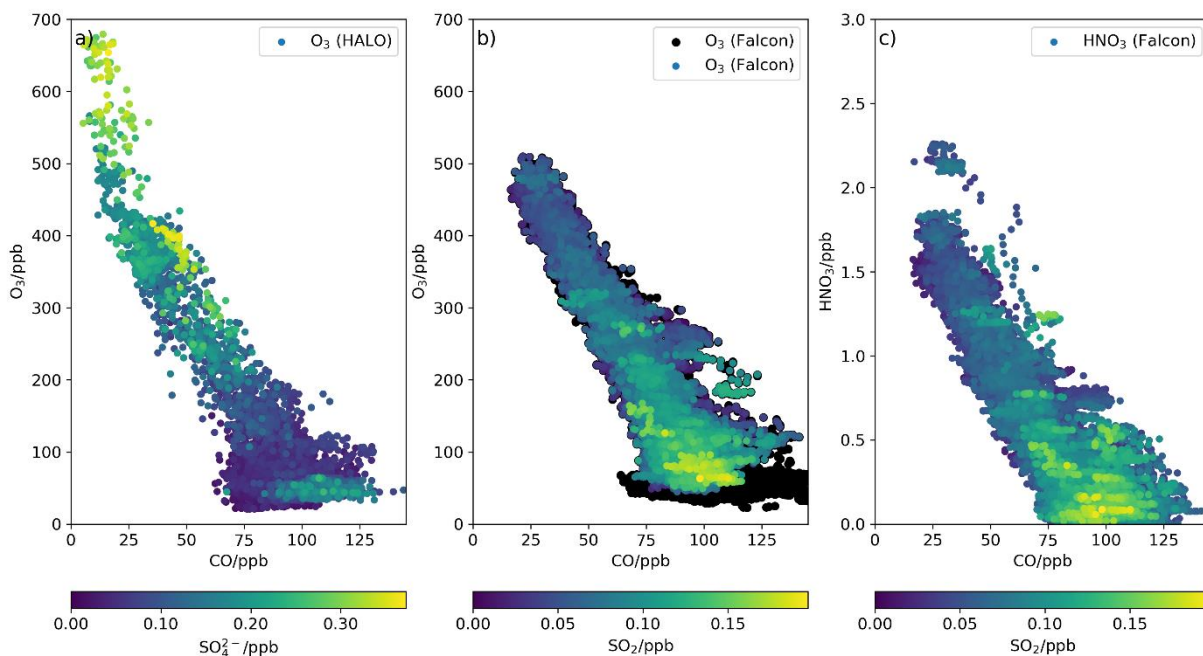
In Figure 3c the profile of the ratio of  $\text{SO}_4^{2-} / (\text{SO}_2 + \text{SO}_4^{2-})$  is plotted. The ratio is a measure of the relative contribution from the precursor  $\text{SO}_2$  to the total sulfur budget. Below the chemical tropopause most of the  $\text{SO}_2$  is still present as  $\text{SO}_2$ , while above the tropopause  $\text{SO}_4^{2-}$  dominates the ratio. The sum of  $\text{SO}_2$  and  $\text{SO}_4^{2-}$  for the median profiles is rather stable around 190 0.10 ppb between 310 K and 340 K, above the sum increases up to on average 0.20 ppb and is dominated by the



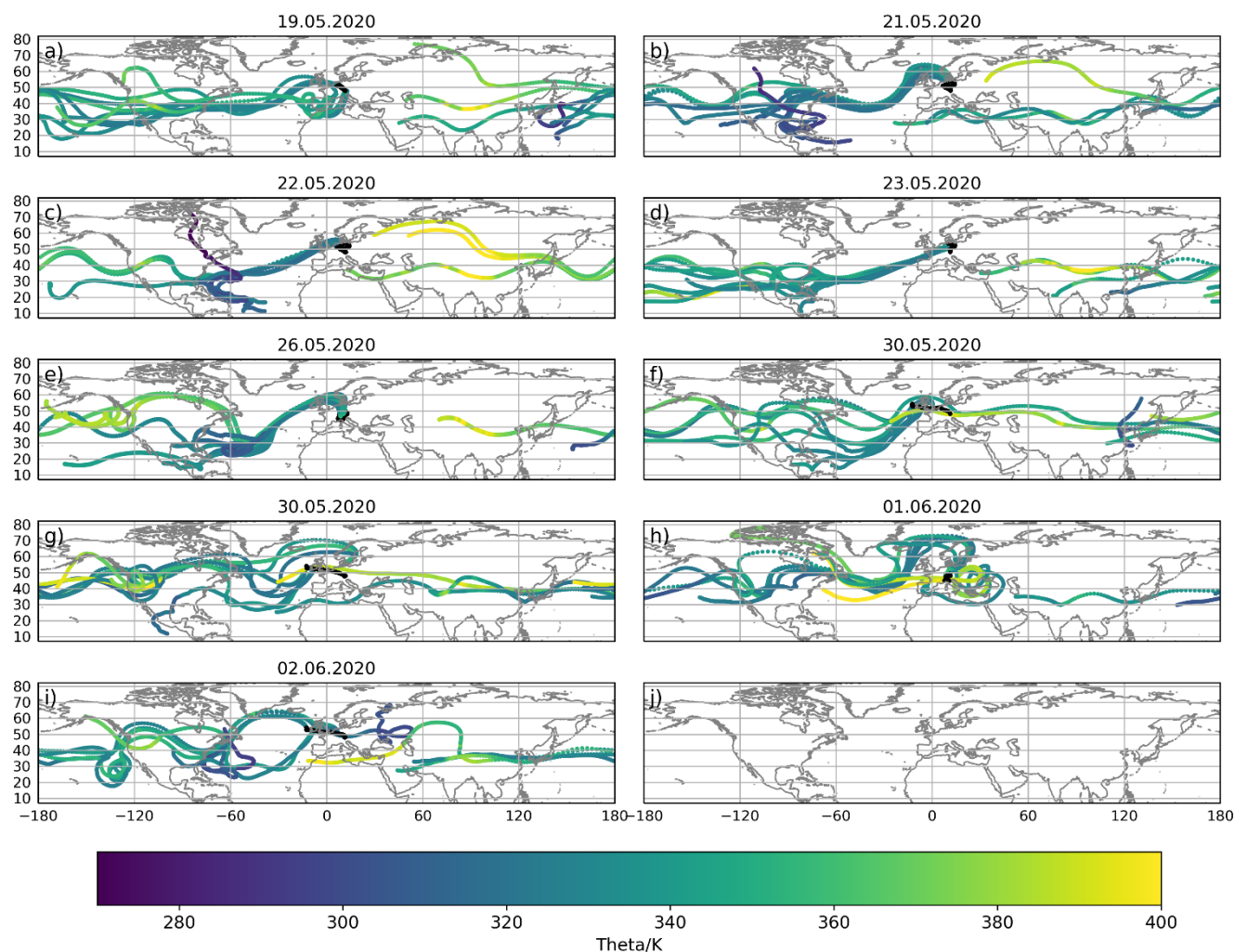
enhancement of  $\text{SO}_4^{2-}$  in the range 340–355 K. In the next section we will discuss potential sources explaining the distribution of sulfur compounds in the UTLS.

### 3.3 Stratospheric and tropospheric influenced air masses

In order to obtain an overview on the distribution of sulfur compounds with respect to the chemical tropopause, Fig. 4 shows tracer-tracer correlations of  $\text{O}_3$ , CO, and  $\text{HNO}_3$ , comparable to previous studies investigating the cross-tropopause exchange and the chemical composition of the tropopause (Fischer et al., 2000; Hoor et al., 2002). In contrast to the median profiles in the previous section, here all available data are plotted, either for HALO (considering  $\text{SO}_4^{2-}$ ) or for Falcon (considering  $\text{SO}_2$ ). In the correlation plot between  $\text{O}_3$  and CO color-coded with  $\text{SO}_4^{2-}$  (Fig. 4a) from HALO for the whole altitude range (0–14 km), the stratospheric branch is visible with low CO and high  $\text{O}_3$  values, while the tropospheric branch is characterised by low  $\text{O}_3$  and high CO values, similar to e.g. Fischer et al., (2000). The transition layer is clearly visible, the layer is a mixing layer, influenced by air masses with stratospheric and tropospheric origin (Hoor et al., 2002). Without the exchange processes across the tropopause, we would expect a L-shape profile (Fischer et al., 2000). The mixing layer almost extends over the whole  $\text{O}_3$  range from 150 ppb to 400 ppb. The higher  $\text{SO}_4^{2-}$  mixing ratios are either in the (unmixed) stratospheric branch or partly mixed into in the upper part of the transition layer. With respect to the chemical tropopause, the elevated  $\text{SO}_4^{2-}$  mixing ratios appear only in the stratosphere ( $\text{O}_3 \geq 120$  ppb; Thouret et al., 2006). In Figure 4b) the correlation between  $\text{O}_3$  and CO with and without color-coded  $\text{SO}_2$  onboard Falcon is displayed. A subset of the Falcon flights is missing there due to missing  $\text{O}_3$  data in the beginning of the campaign. As the Falcon mainly operated up to 12 km, the pure stratospheric branch is hard to identify, while the tropospheric branch is clearly identifiable with the black dots (without  $\text{SO}_2$ ). However, within the mixing layer, the stratospheric and tropospheric influences still differ, which is reflected in the  $\text{SO}_2$  mixing ratios. In order to cover all Falcon flights, we use here  $\text{HNO}_3$  as a stratospheric tracer. In Figure 4c, the  $\text{HNO}_3$  to CO correlation for the measurements onboard Falcon are plotted with color-coded  $\text{SO}_2$ , the Figure includes all Falcon flights, Figure 4b and 4c show similar patterns for  $\text{SO}_2$ , with higher mixing ratios towards more tropospheric influence and lower mixing ratios when the stratospheric influence dominates. Some  $\text{SO}_2$  outliers with higher mixing ratios at enhanced  $\text{HNO}_3$  and reduced CO can be identified. A possible explanation could be (aged) aircraft plume encounters (as observed e.g. in Jurkat et al., 2011), as HYSPILT back trajectory calculations tend towards long range transport in the UTLS region for these cases (Fig. 5). Furthermore, the trajectories do not indicate transport from local PBL sources. Additionally, Hamryszczak et al. (2022) found that hydrogen peroxides were scavenged by clouds during BLUESKY in the lower and middle troposphere (0–7 km). As  $\text{SO}_2$  can easily be scavenged by clouds (Seinfeld and Pandis, 2006), the potential for  $\text{SO}_2$  being transported from the local PBL to the UT seems unlikely. The tracer-tracer-correlation and the relative distribution of  $\text{SO}_2$  along the transition layer show no direct link to the  $\text{SO}_4^{2-}$  distribution, as they are in different regimes, thus we assume that they originate from different sources.



225 **Figure 4: Tracer-tracer correlation for a) 30 sec data CO - O<sub>3</sub> with color-coded SO<sub>4</sub><sup>2-</sup> from HALO flights, b) CO - O<sub>3</sub> in black for whole altitude range, and with color-coded SO<sub>2</sub> (above 8 km) from Falcon flight, when O<sub>3</sub> was available, and c) 1 sec data CO - HNO<sub>3</sub> with color-coded SO<sub>2</sub> from Falcon flights.**



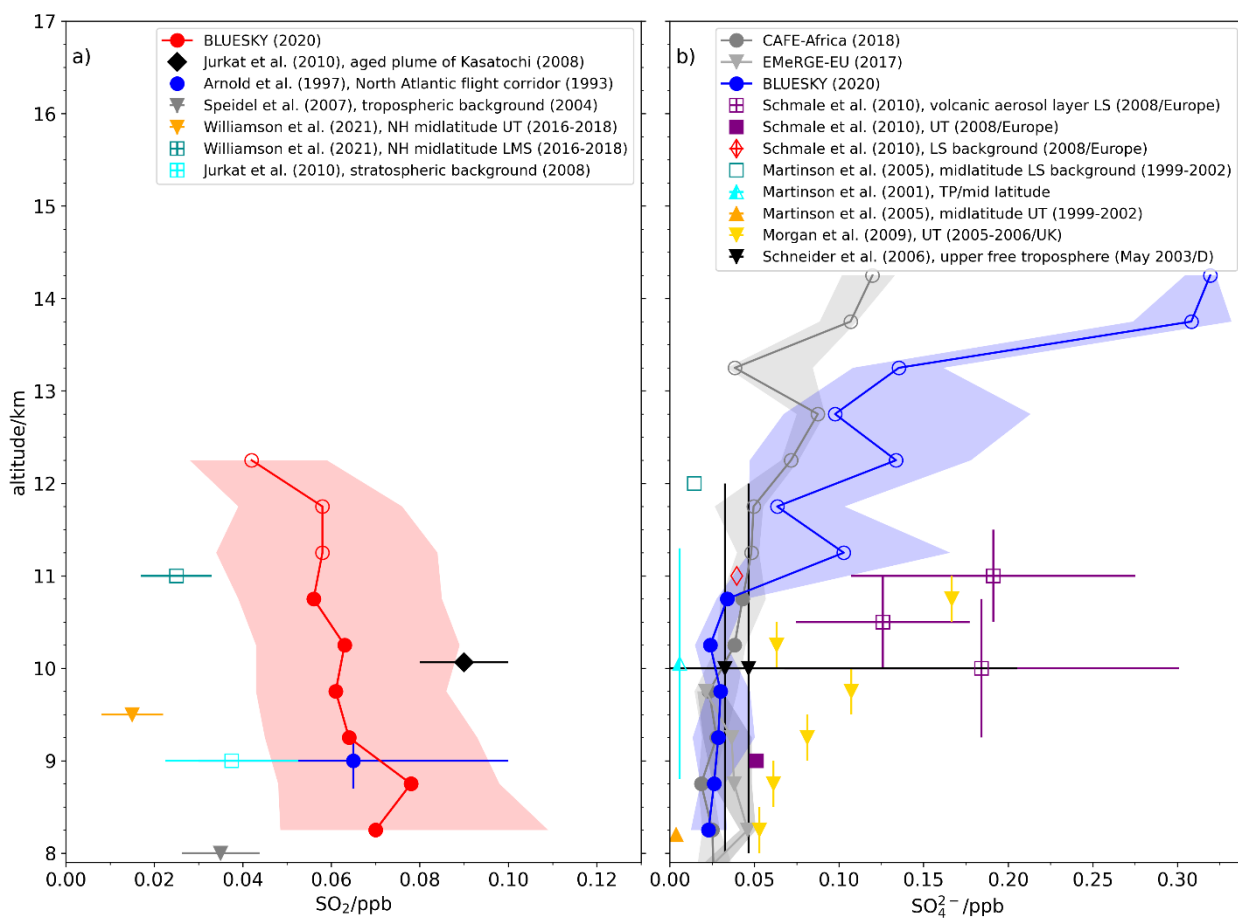
230 **Figure 5:** HYSPLIT 360 hours back trajectories calculated for cases with elevated  $\text{SO}_2$  and  $\text{HNO}_3$  mixing ratios, while  $\text{CO}$  was  
reduced. The release points started in the vicinity of these events. In black are the flight tracks, color-coded is the potential  
temperature along the trajectories to display the transport altitude. Further, some events display transport of PBL air masses with  
origins in Asia, the east coast of the US, or the Caribbean, which is lifted to the UTLS region and then transported at high altitudes  
towards the measurement region. The cases of enhanced  $\text{SO}_2$  were on 19 May 2020 (a), 21 May 2020 (b), 22 May 2020 (c), 23 May  
235 2020 (d), 26 May 2020 (e), 30 May 2020 first flight (f) and second flight (g), 01 June 2020 (h) and 02 June 2020 (i).



#### 4 Enhanced SO<sub>2</sub> in the UT

In Figure 6a, the median SO<sub>2</sub> profile with shaded 25<sup>th</sup> and 75<sup>th</sup> percentile is plotted against the flight altitude, in order to compare the data with literature values. The SO<sub>2</sub> percentiles are calculated for 500 m bins. Similar to Fig. 3b, the median  
240 SO<sub>2</sub> decreases with height from around 0.08 ppb to 0.04 ppb. Previous in situ SO<sub>2</sub> measurements at similar flight altitudes are included in Fig. 6a. Overall, the BLUESKY SO<sub>2</sub> measurements are within the range of previous airborne studies, even though all studies are snapshots of the atmosphere of different locations on the Northern hemisphere, different seasons, and different meteorological situations. Keeping this in mind, we will have a closer look. Williamson et al. (2021) reported low mixing ratios for the remote Northern hemispheric background over the Pacific for the upper troposphere as well as for the  
245 lowermost stratosphere during the ATom mission (2016-2018). Speidel et al. (2007) reported higher SO<sub>2</sub> values for the upper tropospheric background over Europe and the eastern Atlantic in summer 2004. Jurkat et al. (2010) measured the stratospheric background over Europe in autumn 2008 in a similar range to Speidel et al. (2007). Above 12 km the BLUESKY SO<sub>2</sub> mixing ratios agree well with the stratospheric background from Jurkat et al. (2010) and the tropospheric background from Speidel et al. (2007). Surprisingly, the BLUESKY SO<sub>2</sub> profile slightly exceeds the previous measurements  
250 below these altitudes in the upper troposphere. The upper tropospheric SO<sub>2</sub> profile compares better to SO<sub>2</sub> mixing ratios, which were associated with the SO<sub>2</sub> background in the North Atlantic flight corridor in 1997 or 2010 (Arnold et al., 1997; Jurkat et al., 2010). Arnold et al. (1997) reported SO<sub>2</sub> mixing ratios in the range of 0.03-0.3 ppb in October 1993 during POLINAT and Jurkat et al. (2010) measured 0.09 ppb of SO<sub>2</sub> during CONCERT in autumn 2008. Due to implementation of SO<sub>2</sub> emission control policies, the global SO<sub>2</sub> emissions decreased since 1980 (Hoesly et al., 2018; Aas et al., 2019),  
255 nevertheless the sulfur content in kerosene remained unchanged (Lee et al., 2021; Miller et al., 2009), thus the aviation based SO<sub>2</sub> emissions depend on the air traffic.

In 2020, a 72% reduction of the air traffic above Europe has been reported due to the COVID19 lockdown in comparison to the same time period in 2019 (Schumann et al., 2021a, 2021b), hence providing a lower aviation SO<sub>2</sub> source with respect to 2019. Compared to 2010, the 3.5% increase in air traffic per year (Lee et al., 2011) promotes an increase by a factor of 1.5 of  
260 the 2010 air traffic and consequently an increase of 50 percent in aviation SO<sub>2</sub> emissions, given that the sulfur content of the kerosene is unchanged (Lee et al., 2021; Miller et al., 2009). The increase in air traffic might hence in part explain the SO<sub>2</sub> mixing ratios detected in the upper troposphere.



265 **Figure 6: Profiles for a)  $\text{SO}_2$  and b)  $\text{SO}_4^{2-}$  for 500m altitude bins. In a) additional literature  $\text{SO}_2$  values are shown, while in b) literature values for  $\text{SO}_4^{2-}$  are added, including  $\text{SO}_4^{2-}$  profiles from previous HALO missions with the aerosol mass spectrometer C-ToF-AMS onboard: EMERGE-EU in June/July 2017 (Andrés Hernández et al., 2021) and four flights over Europe of the CAFE-Africa mission in July-September 2018. Full markers are tropospheric origin and open markers are stratospheric origin.**

270 In addition, further sources could have contributed to the  $\text{SO}_2$  budget in the upper troposphere.  $\text{SO}_2$  emissions from anthropogenic and natural sources in the PBL can be lifted to the UT via convection or via warm conveyor belts and transported to the measurement region. Arnold et al. (1997) reported an extended layer of enhanced  $\text{SO}_2$  with maxima of up to 3 ppb in the Northeast Atlantic, which was an air mass uplifted and transported from the polluted PBL from the eastern United States. Another possibility is the uplift of polluted air masses from East Asia via warm conveyor belts and upper

275 tropospheric long-range transport towards Europe (Fiedler et al., 2009). Further, the Asian monsoon also serves as a vertical transport pathway for emissions from the PBL up to high altitudes, where the air mass can enter the LS and horizontally be



transported either eastwards (Vogel et al., 2014, 2016) or can be horizontally transported in the UT (Tomsche et al., 2019) and finally reach Europe. Trajectory analysis (Fig 5) for the BLUESKY period indicate some events of PBL air masses with origins in Asia, the east coast of the US, or the Caribbean lifted to the UTLS region and then being transported at high altitudes. Hence, long range transport of SO<sub>2</sub> enriched PBL air masses could have contributed to the observed BLUESKY SO<sub>2</sub> mixing ratios in the UT. Nevertheless, the decrease of SO<sub>2</sub> in the LS, as expected, does not support transport of SO<sub>2</sub> beyond the UT into the LS neither via convection nor warm conveyor belts.

Beside the sources, also sinks of SO<sub>2</sub> can alter the SO<sub>2</sub> concentrations in the UTLS. Beside the conversion to H<sub>2</sub>SO<sub>4</sub>, leading to sulfate particles, SO<sub>2</sub> is removed from the atmosphere by wet and dry deposition. SO<sub>2</sub> can be scavenged by clouds, which lead to a significant reduction of the SO<sub>2</sub> lifetime (Lelieveld, 1993). Furthermore, elevated humidity favours the faster conversion of SO<sub>2</sub> to SO<sub>3</sub> and sulfate, as water vapour enhances the potential for elevated OH concentrations (Pandis and Seinfeld, 2006). As reported by Schumann et al. (2021a, 2021b) the UTLS was drier in spring 2020 in Europe in comparison to previous years. Van Heerwaarden et al. (2021) describe the meteorology in spring 2020 as exceptionally dry and with a lower cloud fraction in comparison to the mean 2010-2019 period over Europe. Less cloud processing would reduce SO<sub>2</sub> sinks. Moreover, lower OH concentrations during BLUESKY period would imply less chemical processing and hence would also reduce SO<sub>2</sub> sinks. Less SO<sub>2</sub> sinks could lead to an enhanced SO<sub>2</sub> lifetime in the UTLS.

In sum, the enhanced SO<sub>2</sub> mixing ratios at cruise levels in Europe in spring 2020 can possibly be explained by a non-negligible aviation SO<sub>2</sub> contribution, WCB or convective transport from the boundary layer and the prolonged SO<sub>2</sub> lifetime caused by the unusually dry UTLS conditions. Beyond that, we are not able to analyse in more detail the different amounts of the aforementioned factors and how they contribute to single flights.

## 5 Stratospheric sulfate aerosol

As mentioned in section 3.2, SO<sub>4</sub><sup>2-</sup> has a distinct profile with a steep increase at a potential temperature of 340 K, which refers here to around 11 km with respect to altitude (Fig. 6b). Up to this altitude, the mixing ratio is rather constant, then it increases. Between 8-11 km O<sub>3</sub> mixing ratios are stable, and above O<sub>3</sub> increases. O<sub>3</sub> mixing ratio above 120 ppb indicates stratospheric air masses as mentioned above, thus the higher SO<sub>4</sub><sup>2-</sup> mixing ratios above 11 km can be attributed to the stratosphere and hence associated with stratospheric aerosol. The layer between 11 and 13.5 km can be influenced from the stratosphere as well as the troposphere, as the data are averaged over a few weeks and varying meteorological conditions, which lead to a broadening of the 25<sup>th</sup> to 75<sup>th</sup> percentiles range.

Previous studies investigate the sulfate aerosol in the UTLS region in northern hemispheric midlatitudes. The BLUESKY mixing ratios in the UT agree well with the observations by Schneider et al. (2006) during May 2003, which were partly influenced by aircraft exhaust plumes. The BLUESKY mixing ratios are lower than the UT background reported by Schmale



et al. (2010). Martinson et al. (2001, 2005) observed significantly lower  $\text{SO}_4^{2-}$  mixing ratios in the European upper troposphere and tropopause region. The  $\text{SO}_4^{2-}$  profile (Morgan et al., 2009) obtained from April 2005 to September 2006 over the UK shows higher  $\text{SO}_4^{2-}$  concentrations compared to the BLUESKY measurements. Morgan et al. (2009) suggest  
310 that the elevated mixing ratios in the UT are the result of regional uplift of polluted air masses during stagnant meteorological conditions over the UK.

Sulfate was measured in two previous HALO missions with the aerosol mass spectrometer C-ToF-AMS in a similar altitude range and region. During EMeRGe-EU, seven research flights were conducted in June/July 2017 above Europe at altitudes up to 10 km (Andrés Hernández et al., 2021). The  $\text{SO}_4^{2-}$  mixing ratio was on average ( $0.04 \pm 0.01$ ) ppb and compares well to  
315 the BLUESKY  $\text{SO}_4^{2-}$  mean in the same altitude range below 10 km. The second HALO mission was CAFE-Africa in summer 2018 and reached altitudes up to 14 km. Here, only data obtained over Europe ( $38^\circ - 57^\circ\text{N}$  and  $14^\circ\text{W} - 16^\circ\text{E}$ ) are used for the comparison, which include two test flights and the ferry flights (27 July, 01 Aug, 07 Aug, and 07 Sept 2018; Voigt et al., 2022). For the altitude range 8-11 km, the  $\text{SO}_4^{2-}$  mean was ( $0.03 \pm 0.01$ ) ppb, similar to the BLUESKY value. Above 11 km in the lower stratosphere,  $\text{SO}_4^{2-}$  raises to ( $0.09 \pm 0.03$ ) ppb. Considering heights above the tropopause, i.e. with  
320 enhanced  $\text{SO}_4^{2-}$  mixing ratios, the stratospheric BLUESKY  $\text{SO}_4^{2-}$  concentrations are a factor of 2 to 3 higher than the observations in summer 2018.

In the following, we investigate the origin of the elevated stratospheric  $\text{SO}_4^{2-}$  mixing ratios during BLUESKY. One major source of  $\text{SO}_4^{2-}$  in the stratosphere are volcanic eruptions. One year before BLUESKY, the volcano Raikoke on the Kuril Islands (Russia,  $48.29^\circ\text{N}$ ,  $153.25^\circ\text{E}$ ) in the Western Pacific started to erupt on 21 June 2019 and continued for some days, it  
325 was categorised to volcanic explosivity index  $\text{VEI} \geq 4$ . Several explosive eruptions emitted a dense ash and  $\text{SO}_2$  plume, which rose up to 19 km and 20 km on consecutive days (Hedelt et al., 2019), thus also injecting into the stratosphere. Based on TROPOMI analysis de Leeuw et al. (2021) reported, that the eruption released 1.4-1.6 Tg  $\text{SO}_2$  into the atmosphere and simulated also that approximately 0.9-1.1 Tg  $\text{SO}_2$  thereof were injected into the stratosphere. Kloss et al. (2021) used satellite based OMPS (Ozone Mapping Profiler Suite Limb Profiler) stratospheric Aerosol Optical Depth (sAOD) to  
330 investigate the temporal evolution from before the Raikoke eruption until May 2020. Almost one year later, the sAOD was still higher than prior to the eruption. This suggests that elevated  $\text{SO}_4^{2-}$  measured in the stratosphere during BLUESKY was partly caused by the Raikoke eruption a year earlier. The eruption of Mount St Helens in 1980 was of comparable size, midlatitude location, and  $\text{SO}_2$  emissions (Deshler et al., 2006) and its impact was also visible for almost a year. Still, other sources cannot be completely ruled out. For example, severe wildfires in Alberta/Canada developed pyro cumulus clouds in  
335 June 2019. The biomass burning emissions were uplifted into the lower stratosphere (Osborne et al., 2022). In July 2019, also severe fires in Siberia/Russia impacted the OPMS sAOD (Kloss et al., 2021). In comparison to the Raikoke eruption, these biomass burning contributions are of lower magnitude. Reifenberg et al. (2021) suggest that other small and medium sized volcanic eruptions from tropical latitudes, could have reached the stratosphere and thus impacted the stratospheric aerosol over Europe. One example is the volcano Taal on the Philippines ( $14.00^\circ\text{N}$ ,  $120.99^\circ\text{E}$ ), which erupted on 12 January





340 2020, and its ash and gas plume rose up to around 10-15 km height (Global Volcanism Program, 2020. Report on Taal (Philippines)). The VEI was estimated to 3 and the SO<sub>2</sub> emissions estimated to 0.019 Tg (Liu et al., 2020). According to simulations of Reifenberg et al. (2021), the Taal eruption lead partly to an increase of SO<sub>4</sub><sup>2-</sup> in the LS during BLUESKY.

The measured SO<sub>4</sub><sup>2-</sup> mixing ratios in the LS agree with other volcano related in situ studies. The highest mixing ratios are reported by Schmale et al. (2010). They probed layers with enhanced SO<sub>4</sub><sup>2-</sup> in October/November 2008 roughly 3 months  
345 after the eruption of Mount Kasatochi (erupted 08 August 2008, 52.18°N, 175.51°W, 1.5 Tg SO<sub>2</sub>), with an injection height reaching into the stratosphere and additionally Mount Okmok (53.40°N, 168.17°W) erupted on 12 July 2008 (0.2 Tg SO<sub>2</sub>, Carn et al., 2008). Jurkat et al. (2010) also measured enhanced SO<sub>2</sub> concentrations in the stratosphere in the 3 months-old Kasatochi plume during the CONCERT campaign (Voigt et al., 2010). Martinsson et al. (2009) reported particulate sulfur concentrations shortly after the Kasatochi eruption were 10 times higher than before the eruption and even 3-4 months after  
350 the eruption they were enhanced by a factor of 3. In contrast, during volcanic quiescent periods, like the period between 1997 and 2008 (Deshler, 2008) the SO<sub>4</sub><sup>2-</sup> has reduced mixing ratios in the stratosphere, and Martinson et al. (2005) reported SO<sub>4</sub><sup>2-</sup> mixing ratios of 0.01 ppb for the lower stratosphere for the years 1999-2002.

The enhanced SO<sub>2</sub> in the UT as described in section 4 and the longer SO<sub>2</sub> lifetime could possibly have a minor effect on the stratospheric sulfate aerosol. In these conditions, the SO<sub>2</sub> had more time to be transported into the LS and finally be  
355 transformed to SO<sub>4</sub><sup>2-</sup>, adding to the SO<sub>4</sub><sup>2-</sup> mixing ratios. Moreover, OCS is transported within the Brewer Dobson Circulation from the upper stratosphere to the lower stratosphere and being transformed via SO<sub>2</sub> to H<sub>2</sub>SO<sub>4</sub>. According to Brühl et al. (2012), it is the most important source for maintaining the stratospheric aerosol layer in volcanic quiescent periods and also for BLUESKY, OCS oxidation adds to the stratospheric SO<sub>4</sub><sup>2-</sup> background to some extent.

## 6 Conclusion and outlook

360 We find elevated SO<sub>4</sub><sup>2-</sup> mixing ratios in stratospheric air masses, and enhanced SO<sub>2</sub> mixing ratios in tropospheric air masses over Central Europe and the North Atlantic in spring 2020. The elevated SO<sub>2</sub> of 0.06 ppb in the UT agrees with SO<sub>2</sub> mixing ratios performed in the background of the North Atlantic flight corridor in 2008 (Jurkat et al., 2010) despite lower air traffic due to COVID-19 restrictions in 2020. The 3.5% increase in air traffic since 2010 in part compensates the air traffic reduction in 2020. In addition, exceptional dry weather conditions leading to a low cloud fraction and low OH concentrations in the  
365 UTLS in May 2020 (Schumann et al., 2021a, 2021b, Van Heerwaarden et al., 2021) reduced SO<sub>2</sub> sinks and increased SO<sub>2</sub> lifetime. Other boundary layer SO<sub>2</sub> sources from convective or WCB transport could have contributed to a small extend. In the LS, enhanced SO<sub>4</sub><sup>2-</sup> mixing ratios were observed. In comparison to previous studies the SO<sub>4</sub><sup>2-</sup> mixing ratios were clearly above SO<sub>4</sub><sup>2-</sup> mixing ratios reported during volcanic quiescent periods (e.g. Martinson et al., 2001, 2005) and agreed with SO<sub>4</sub><sup>2-</sup> mixing ratios in volcanic impacted air masses (e.g. Schmale et al., 2010) measured at altitudes below 12 km. Compared to  
370 2018, stratospheric SO<sub>4</sub><sup>2-</sup> was significantly enhanced in 2020. The eruption of the volcano Raikoke injected 0.9-1.1 Tg of



375 SO<sub>2</sub> into the stratosphere (de Leeuw et al., 2021) in June 2019. In May 2020, an enhanced sAOD still was observed by Kloss et al. (2021) in the northern hemisphere caused by the Raikoke eruption and to a smaller extent by severe biomass burning events from June/July 2019 in Siberia and Canada. Further, Reifenberg et al. (2021) found that the eruption of the tropical volcano Taal in January 2020 contributed to the enhanced SO<sub>4</sub><sup>2-</sup> in the LS. We suggest these to be the primary sources of the enhanced stratospheric SO<sub>4</sub><sup>2-</sup> concentrations measured during BLUESKY.

Overall, the unprecedented BLUESKY mission was conducted during exceptional meteorological conditions and also reduced air traffic, both impacted the SO<sub>2</sub> mixing ratios in the UT due to changes in the emissions and also sinks. The enhanced stratospheric sulfate aerosol, which was observed, was likely impacted by the volcano Raikoke, and smaller sources. Together with the observations of other sulfur compounds such as gaseous H<sub>2</sub>SO<sub>4</sub> on HALO, which are still under evaluation, 380 the unique and comprehensive data set of sulfur compounds allows to test our understanding of the sulfur chemistry in global models (Reifenberg et al., 2021).

In a broader context, the present results give new insights in the sulfur chemistry in the UTLS region with respect to limited sources and sinks. They help to better understand a) the sensitivity of SO<sub>2</sub> to missing sinks and b) the stratospheric aerosol and its dependence on perturbances and their lasting impacts. Both aspects are important to improve models, especially with respect 385 to simulations of the Earth's radiation budget, because changes in the radiation balance in the UTLS impact feedback processes in the global climate.

### Data availability

Data are available on request at the HALO data base at <https://halo-db.pa.op.dlr.de/mission/119>.

### 390 Author contribution

CV, TJW, HS, JL planned the flight experiment. AM, JL, KK, JS, MS, LR performed the in-flight measurements. KK and JS provided evaluated particulate data and previous campaign data and supported the analysis. AM provided supporting evaluation and assisted the analysis. FO, AZ, HF, LR provided supporting evaluation. SK supported the analysis. LT evaluated and analysed the data and prepared the manuscript with contributions from CV, AM, TJW, JS, KK, HF and SK. All co-authors 395 commented on the manuscript.



## Competing interests

The authors declare that they have no conflict of interest.

## Acknowledgements

Laura Tomsche is funded by the Deutsche Forschungsgemeinschaft (DFG, German Research Foundation) – TRR 301 –  
400 Project-ID 428312742. The HALO flights during the BLUESKY mission were funded by the Max Planck Society. The authors  
gratefully acknowledge the NOAA Air Resources Laboratory (ARL) for the provision of the HYSPLIT transport and  
dispersion model and/or READY website (<https://www.ready.noaa.gov>) used in this publication.

## References

- 405 Aas, W., Mortier, A., Bowersox, V., Cherian, R., Faluvegi, G., Fagerli, H., Hand, J., Klimont, Z., Galy-Lacaux, C., Lehmann, C. M. B.,  
Myhre, C. L., Myhre, G., Olivie, D., Sato, K., Quaas, J., Rao, P. S. P., Schulz, M., Shindell, D., Skeie, R. B., Stein, A., Takemura,  
T., Tsyro, S., Vet, R., Xu, X. (2019). Global and regional trends of atmospheric sulfur. *Scientific Reports*, 9(1), 953.  
doi:10.1038/s41598-018-37304-0
- 410 Almeida, J., Schobesberger, S., Kürten, A., Ortega, I. K., Kupiainen-Määttä, O., Praplan, A. P., Adamov, A., Amorim, A., Bianchi, F.,  
Breitenlechner, M., David, A., Dommen, J., Donahue, N. M., Downard, A., Dunne, E., Duplissy, J., Ehrhart, S., Flagan, R. C.,  
Franchin, A., Guida, R., Hakala, J., Hansel, A., Heinritzi, M., Henschel, H., Jokinen, T., Junninen, H., Kajos, M., Kangasluoma,  
J., Keskinen, H., Kupc, A., Kurtén, T., Kvashin, A. N., Laaksonen, A., Lehtipalo, K., Leiminger, M., Leppä, J., Loukonen, V.,  
Makmutov, V., Mathot, S., McGrath, M. J., Nieminen, T., Olenius, T., Onnela, A., Petäjä, T., Riccobono, F., Riipinen, I.,  
415 Rissanen, M., Rondo, L., Ruuskanen, T., Santos, F. D., Sarnela, N., Schallhart, S., Schnitzhofer, R., Seinfeld, J. H., Simon, M.,  
Sipilä, M., Stozhkov, Y., Stratmann, F., Tomé, A., Tröstl, J., Tsagkogeorgas, G., Vaattovaara, P., Viisanen, Y., Virtanen, A.,  
Vrtala, A., Wagner, P. E., Weingartner, E., Wex, H., Williamson, C., Wimmer, D., Ye, P., Yli-Juuti, T., Carslaw, K. S., Kulmala,  
M., Curtius, J., Baltensperger, U., Worsnop, D. R., Vehkamäki, H., Kirkby, J. (2013). Molecular understanding of sulphuric acid-  
amine particle nucleation in the atmosphere. *Nature*, 502(7471), 359-363. doi:10.1038/nature12663
- 420 Andrés Hernández, M. D., Hilboll, A., Ziereis, H., Förster, E., Krüger, O. O., Kaiser, K., Schneider, J., Barnaba, F., Vrekoussis, M., Schmidt,  
J., Huntrieser, H., Blechschmidt, A. M., George, M., Nenakhov, V., Klausner, T., Holanda, B. A., Wolf, J., Eirenschmalz, L.,  
Krebsbach, M., Pöhlker, M. L., Hedegaard, A. B., Mei, L., Pfeilsticker, K., Liu, Y., Koppmann, R., Schlager, H., Bohn, B.,  
Schumann, U., Richter, A., Schreiner, B., Sauer, D., Baumann, R., Mertens, M., Jöckel, P., Kilian, M., Stratmann, G., Pöhlker, C.,  
Campanelli, M., Pandolfi, M., Sicard, M., Gomez-Amo, J. L., Pujadas, M., Bigge, K., Kluge, F., Schwarz, A., Daskalakis, N.,  
425 Walter, D., Zahn, A., Pöschl, U., Bönisch, H., Borrmann, S., Platt, U., Burrows, J. P. (2021). Overview: On the transport and  
transformation of pollutants in the outflow of major population centres - observational data from the EMERG European intensive  
operational period in summer 2017. *Atmos. Chem. Phys. Discuss.*, 2021, 1-81. doi:10.5194/acp-2021-500
- Arnold, F., Schneider, J., Gollinger, K., Schlager, H., Schulte, P., Hagen, D. E., Whitefield, P. D., van Velthoven, P. (1997). Observation of  
upper tropospheric sulfur dioxide- and acetone-pollution: Potential implications for hydroxyl radical and aerosol formation.  
*Geophysical Research Letters*, 24(1), 57-60. doi:10.1029/96gl03693
- 430 Brock, C., Hamill, P., Wilson, J., Jonsson, H., & Chan, K. J. S. (1995). Particle formation in the upper tropical troposphere: A source of  
nuclei for the stratospheric aerosol. *270*(5242), 1650-1653.
- Brühl, C., Lelieveld, J., Crutzen, P. J., Tost, H. (2012). The role of carbonyl sulphide as a source of stratospheric sulphate aerosol and its  
impact on climate. *Atmos. Chem. Phys.*, 12(3), 1239-1253. doi:10.5194/acp-12-1239-2012
- 435 Carn, S., Krotkov, N., Fioletov, V., Yang, K., Krueger, A., & Tarasick, D. (2008). *Emission, transport and validation of sulfur dioxide in  
the 2008 Okmok and Kasatochi eruption clouds*. Paper presented at the AGU Fall Meeting Abstracts.
- Clarisse, L., Fromm, M., Ngadi, Y., Emmons, L., Clerbaux, C., Hurtmans, D., & Coheur, P.-F. (2011). Intercontinental transport of  
anthropogenic sulfur dioxide and other pollutants: An infrared remote sensing case study. *Geophysical Research Letters*, 38(19),  
doi:<https://doi.org/10.1029/2011GL048976>



- 440 Crutzen, P. J. (2006). Albedo enhancement by stratospheric sulfur injections: a contribution to resolve a policy dilemma? *Climatic change*, 77(3-4), 211.
- Cziczo, D. J., Thomson, D. S., & Murphy, D. M. (2001). Ablation, Flux, and Atmospheric Implications of Meteors Inferred from Stratospheric Aerosol. *Science*, 291(5509), 1772-1775. doi:10.1126/science.1057737
- de Leeuw, J., Schmidt, A., Witham, C. S., Theys, N., Taylor, I. A., Grainger, R. G., Pope, R. J., Haywood, J., Osborne, M., Kristiansen, N. I. (2021). The 2019 Raikoke volcanic eruption – Part 1: Dispersion model simulations and satellite retrievals of volcanic sulfur dioxide. *Atmos. Chem. Phys.*, 21(14), 10851-10879. doi:10.5194/acp-21-10851-2021
- 445 Deshler, T., Anderson-Sprecher, R., Jäger, H., Barnes, J., Hofmann, D. J., Clemesha, B., Simonich, D., Osborn, M., Grainger, R. G., Godin-Beekmann, S. (2006). Trends in the nonvolcanic component of stratospheric aerosol over the period 1971–2004. *111(D1)*. doi:<https://doi.org/10.1029/2005JD006089>
- 450 Deshler, T. J. A. R. (2008). A review of global stratospheric aerosol: Measurements, importance, life cycle, and local stratospheric aerosol. *90(2-4)*, 223-232.
- Drewnick, F., Hings, S. S., DeCarlo, P., Jayne, J. T., Gonin, M., Fuhrer, K., Weimer, S., Jimenez, J. L., Demerjian, K. L., Borrmann, S., Worsnop, D. R. (2005). A New Time-of-Flight Aerosol Mass Spectrometer (TOF-AMS)—Instrument Description and First Field Deployment. *Aerosol Science and Technology*, 39(7), 637-658. doi:10.1080/02786820500182040
- 455 English, J. M., Toon, O. B., Mills, M. J., & Yu, F. (2011). Microphysical simulations of new particle formation in the upper troposphere and lower stratosphere. *Atmos. Chem. Phys.*, 11(17), 9303-9322. doi:10.5194/acp-11-9303-2011
- Fiedler, V., Nau, R., Ludmann, S., Arnold, F., Schlager, H., & Stohl, A. (2009). East Asian SO<sub>2</sub> pollution plume over Europe & Part 1: Airborne trace gas measurements and source identification by particle dispersion model simulations. *Atmos. Chem. Phys.*, 9(14), 4717-4728. doi:10.5194/acp-9-4717-2009
- 460 Fischer, H., Wienhold, F. G., Hoor, P., Bujok, O., Schiller, C., Siegmund, P., Ambaum, M., Scheeren, H. A., Lelieveld, J. (2000). Tracer correlations in the northern high latitude lowermost stratosphere: Influence of cross-tropopause mass exchange. *Geophysical Research Letters*, 27(1), 97-100. doi:<https://doi.org/10.1029/1999GL010879>
- Fromm, M., Bevilacqua, R., Servranckx, R., Rosen, J., Thayer, J. P., Herman, J., & Larko, D. (2005). Pyro-cumulonimbus injection of smoke to the stratosphere: Observations and impact of a super blowup in northwestern Canada on 3–4 August 1998. *110(D8)*. doi:<https://doi.org/10.1029/2004JD005350>
- 465 Fueglistaler, S., Dessler, A., Dunkerton, T., Folkins, I., Fu, Q., & Mote, P. W. (2009). Tropical tropopause layer. *Reviews of Geophysics*, 47(1).
- Gottschaldt, K. D., Schlager, H., Baumann, R., Bozem, H., Eyring, V., Hoor, P., Jöckel, P., Jurkat, T., Voigt, C., Zahn, A., Ziereis, H. (2017). Trace gas composition in the Asian summer monsoon anticyclone: a case study based on aircraft observations and model simulations. *Atmos. Chem. Phys.*, 17(9), 6091-6111. doi:10.5194/acp-17-6091-2017
- 470 Gottschaldt, K. D., Schlager, H., Baumann, R., Cai, D. S., Eyring, V., Graf, P., Grewe, V., Jöckel, P., Jurkat-Witschas, T., Voigt, C., Zahn, A., Ziereis, H. (2018). Dynamics and composition of the Asian summer monsoon anticyclone. *Atmos. Chem. Phys.*, 18(8), 5655-5675. doi:10.5194/acp-18-5655-2018
- Hamryszczak, Z. T., Pozzer, A., Obersteiner, F., Bohn, B., Steil, B., Lelieveld, J., & Fischer, H. (2022). Distribution of hydrogen peroxide over Europe during the BLUESKY aircraft campaign. *Atmos. Chem. Phys. Discuss.*, 2022, 1-28. doi:10.5194/acp-2022-89
- 475 Hedelt, P., Efremenko, D. S., Loyola, D. G., Spurr, R., & Clarisse, L. (2019). Sulfur dioxide layer height retrieval from Sentinel-5 Precursor/TROPOMI using FP\_ILM. *Atmos. Meas. Tech.*, 12(10), 5503-5517. doi:10.5194/amt-12-5503-2019
- Hoesly, R. M., Smith, S. J., Feng, L., Klimont, Z., Janssens-Maenhout, G., Pitkanen, T., Seibert, J. J., Vu, L., Andres, R. J., Bolt, R. M., Bond, T. C., Dawidowski, L., Kholod, N., Kurokawa, J. I., Li, M., Liu, L., Lu, Z., Moura, M. C. P., O'Rourke, P. R., Zhang, Q. (2018). Historical (1750–2014) anthropogenic emissions of reactive gases and aerosols from the Community Emissions Data System (CEDs). *Geosci. Model Dev.*, 11(1), 369-408. doi:10.5194/gmd-11-369-2018
- 480 Hoor, P., Fischer, H., Lange, L., Lelieveld, J., & Brunner, D. (2002). Seasonal variations of a mixing layer in the lowermost stratosphere as identified by the CO-O<sub>3</sub> correlation from in situ measurements. *Journal of Geophysical Research: Atmospheres*, 107(D5), ACL 1-1-ACL 1-11. doi:<https://doi.org/10.1029/2000JD000289>
- Junge, C. E., Chagnon, C. W., & Manson, J. E. J. o. A. S. (1961). Stratospheric aerosols. *18(1)*, 81-108.
- 485 Jurkat, T., Kaufmann, S., Voigt, C., Schäuble, D., Jeßberger, P., Ziereis, H. (2016). The airborne mass spectrometer AIMS – Part 2: Measurements of trace gases with stratospheric or tropospheric origin in the UTLS. *Atmos. Meas. Tech.*, 9(4), 1907-1923. doi:10.5194/amt-9-1907-2016
- Jurkat, T., Voigt, C., Arnold, F., Schlager, H., Aufmhoff, H., Schmale, J., Schneider, J., Lichtenstern, M., Dörnbrack, A. (2010). Airborne stratospheric ITCIMS measurements of SO<sub>2</sub>, HCl, and HNO<sub>3</sub> in the aged plume of volcano Kasatochi. *Journal of Geophysical Research*, 115. doi:10.1029/2010jd013890
- 490 Jurkat, T., Voigt, C., Arnold, F., Schlager, H., Kleffmann, J., Aufmhoff, H., Schäuble, D., Schaefer, M., Schumann, U. (2011). Measurements of HONO, NO, NO<sub>y</sub> and SO<sub>2</sub> in aircraft exhaust plumes at cruise. *Geophysical Research Letters*, 38(10), n/a-n/a. doi:10.1029/2011gl046884



- 495 Jurkat, T., Voigt, C., Kaufmann, S., Zahn, A., Sprenger, M., Hoor, P., Bozem, H., Müller, S., Dörnbrack, A., Schlager, H., Bönisch, H., Engel, A. (2014). A quantitative analysis of stratospheric HCl, HNO<sub>3</sub>, and O<sub>3</sub> in the tropopause region near the subtropical jet. *Geophysical Research Letters*, 41(9), 3315–3321. doi:10.1002/2013gl059159
- 500 Kirkby, J., Curtius, J., Almeida, J., Schobesberger, S., Kürten, A., Ortega, I. K., Kupiainen-Määttä, O., Praplan, A. P., Adamov, A., Amorim, A., Bianchi, F., Breitenlechner, M., David, A., Dommen, J., Donahue, N. M., Downard, A., Dunne, E., Duplissy, J., Ehrhart, S., Flagan, R., & Dunne, E., Duplissy, J., Ehrhart, S., Franchin, A., Gagné, S., Ickes, L., Kürten, A., Kupc, A., Metzger, A., Riccobono, F., Rondo, L., Schobesberger, S., Tsagkogeorgas, G., Wimmer, D., Amorim, A., Bianchi, F., Breitenlechner, M., David, A., Dommen, J., Downard, A., Ehn, M., Flagan, R. C., Haider, S., Hansel, A., Hauser, D., Jud, W., Junninen, H., Kreissl, F., Kvashin, A., Laaksonen, A., Lehtipalo, K., Lima, J., Lovejoy, E. R., Makhmutov, V., Mathot, S., Mikkilä, J., Minginette, P., Mogo, S., Nieminen, T., Onnela, A., Pereira, P., Petäjä, T., Schnitzhofer, R., Seinfeld, J. H., Sipilä, M., Stozhkov, Y., Stratmann, F., Tomé, A., Vanhanen, J., Viisanen, Y., Vrtala, A., Wagner, P. E., Walther, H., Weingartner, E., Wex, H., Winkler, P. M., Carslaw, K. S., Worsnop, D. R., Baltensperger, U., Kulmala, M. (2011). Role of sulphuric acid, ammonia and galactic cosmic rays in atmospheric aerosol nucleation. *Nature*, 476(7361), 429–433. doi:10.1038/nature10343
- 505 Klausner, T., Mertens, M., Huntrieser, H., Galkowski, M., Kuhlmann, G., Baumann, R., Fiehn, A., Jöckel, P., Pühl, M., Roiger, A. (2020). Urban greenhouse gas emissions from the Berlin area: A case study using airborne CO<sub>2</sub> and CH<sub>4</sub> in situ observations in summer 2018. *Elementa: Science of the Anthropocene*, 8. doi:10.1525/elementa.411
- 510 Kloss, C., Berthet, G., Sellitto, P., Ploeger, F., Taha, G., Tidiga, M., Eremenko, M., Bossolasco, A., Jégou, F., Renard, J.-B., Legras, B. (2021). Stratospheric aerosol layer perturbation caused by the 2019 Raikoke and Ulawun eruptions and their radiative forcing. *Atmospheric Chemistry and Physics*, 21(1), 535–560. doi:10.5194/acp-21-535-2021
- 515 Kremser, S., Thomason, L. W., von Hobe, M., Hermann, M., Deshler, T., Anderson-Sprecher, R., Jäger, H., Barnes, J., Hofmann, D. J., Clemesha, B., Simonich, D., Osborn, M., Grainger, R. G., Godin-Beekmann, S., Timmreck, C., Toohey, M., Stenke, A., Schwarz, J. P., Weigel, R. (2016). Stratospheric aerosol—Observations, processes, and impact on climate. *J Reviews of Geophysics*, 54(2), 278–335.
- Krippner, J. B., and Venzke, E., eds. (2020). Global Volcanism Program, 2020. Report on Taal (Philippines) *Global Volcanism Program*, 45. doi:<https://doi.org/10.5479/si.GVP.BGVN202006-273070>
- 520 Krüger, O. O., Holanda, B. A., Chowdhury, S., Pozzer, A., Walter, D., Pöhlker, C., Andrés Hernández, M. D., Burrows, J. P., Voigt, C., Lelieveld, J., Quaas, J., Pöschl, U., Pöhlker, M. L. (2022). Black carbon aerosol reductions during COVID-19 confinement quantified by aircraft measurements over Europe. *Atmos. Chem. Phys. Discuss.*, 2022, 1–36. doi:10.5194/acp-2021-1100
- Lee, C., Martin, R. V., van Donkelaar, A., Lee, H., Dickerson, R. R., Hains, J. C., Krotkov, N., Richter, A., Vinnikov, K., Schwab, J. J. (2011). SO<sub>2</sub> emissions and lifetimes: Estimates from inverse modeling using in situ and global, space-based (SCIAMACHY and OMI) observations. *116(D6)*. doi:<https://doi.org/10.1029/2010JD014758>
- 525 Lee, D. S., Fahey, D.W., Skowron, A., Allen, M.R., Burkhardt, U., Chen, Q., Doherty, S.J., Freeman, S., Forster, P.M., Fuglestedt, J. (2021). The contribution of global aviation to anthropogenic climate forcing for 2000 to 2018. *J Atmospheric environment*, 244, 117834.
- Lee, D. S., Pitari, G., Grewe, V., Gierens, K., Penner, J. E., Petzold, A., Prather, M.J., Schumann, U., Bais, A., Berntsen, T. (2010). Transport impacts on atmosphere and climate: Aviation. *J Atmospheric environment*, 44(37), 4678–4734.
- 530 Lelieveld, J. (1993). Multi-phase processes in the atmospheric sulfur cycle. In *Interactions of C, N, P and S biogeochemical cycles and global change* (pp. 305–331): Springer.
- Liu, F., Xing, C., Li, J., Wang, B., Chai, J., Gao, C., Huang, G., Liu, J., Chen, D. (2020). Could the Recent Taal Volcano Eruption Trigger an El Niño and Lead to Eurasian Warming? *Advances in Atmospheric Sciences*, 37(7), 663–670. doi:10.1007/s00376-020-2041-z
- Marsing, A. (2021). *Chlorine Partitioning in the Lowermost Arctic Stratosphere During Winter—an Aircraft in Situ Measurement Perspective*. Johannes Gutenberg-Universität Mainz,
- 535 Marsing, A., Jurkat-Witschas, T., Groß, J. U., Kaufmann, S., Heller, R., Engel, A., Hoor, P., Krause, J., Voigt, C. (2019). Chlorine partitioning in the lowermost Arctic vortex during the cold winter 2015/2016. *Atmos. Chem. Phys.*, 19(16), 10757–10772. doi:10.5194/acp-19-10757-2019
- Martinsson, B. G., Brenninkmeijer, C. A. M., Carn, S. A., Hermann, M., Heue, K.-P., van Velthoven, P. F. J., & Zahn, A. (2009). Influence of the 2008 Kasatochi volcanic eruption on sulfurous and carbonaceous aerosol constituents in the lower stratosphere. *36(12)*. doi:<https://doi.org/10.1029/2009GL038735>
- 540 Martinsson, B. G., Nguyen, H. N., Brenninkmeijer, C. A. M., Zahn, A., Heintzenberg, J., Hermann, M., & van Velthoven, P. F. J. (2005). Characteristics and origin of lowermost stratospheric aerosol at northern midlatitudes under volcanically quiescent conditions based on CARIBIC observations. *110(D12)*. doi:<https://doi.org/10.1029/2004JD005644>
- Martinsson, B. G., Papaspiropoulos, G., Heintzenberg, J., & Hermann, M. J. G. r. l. (2001). Fine mode particulate sulphur in the tropopause region measured from intercontinental flights (CARIBIC). *28(7)*, 1175–1178.
- 545 McCormick, M. P., Thomason, L. W., & Trepte, C. R. J. N. (1995). Atmospheric effects of the Mt Pinatubo eruption. *373(6513)*, 399–404.
- Molleker, S., Helleis, F., Klimach, T., Appel, O., Clemen, H. C., Dragoneas, A., Gurk, C., Hünig, A., Köllner, F., Rubach, F., Schulz, C., Schneider, J., Borrmann, S. (2020). Application of an O-ring pinch device as a constant-pressure inlet (CPI) for airborne sampling. *Atmos. Meas. Tech.*, 13(7), 3651–3660. doi:10.5194/amt-13-3651-2020



- 550 Morgan, W. T., Allan, J. D., Bower, K. N., Capes, G., Crosier, J., Williams, P. I., & Coe, H. (2009). Vertical distribution of sub-micron aerosol chemical composition from North-Western Europe and the North-East Atlantic. *Atmos. Chem. Phys.*, 9(15), 5389-5401. doi:10.5194/acp-9-5389-2009
- Murphy, D., Froyd, K., Schwarz, J., & Wilson, J. J. Q. J. o. t. R. M. S. (2014). Observations of the chemical composition of stratospheric aerosol particles. *140*(681), 1269-1278.
- 555 Nussbaumer, C. M., Pozzer, A., Tadic, I., Röder, L., Obersteiner, F., Harder, H., Lelieveld, J., Fischer, H. (2021). Tropospheric ozone production and chemical regime analysis during the COVID-19 lockdown over Europe. *Atmos. Chem. Phys. Discuss.*, 2021, 1-20. doi:10.5194/acp-2021-1028
- Osborne, M. J., de Leeuw, J., Witham, C., Schmidt, A., Beckett, F., Kristiansen, N., Buxmann, J., Saint, C., Welton, E. J., Fochesatto, J., Gomes, A. R., Bundke, U., Petzold, A., Marengo, F., Haywood, J. (2022). The 2019 Raikoke volcanic eruption – Part 2: Particle-phase dispersion and concurrent wildfire smoke emissions. *Atmos. Chem. Phys.*, 22(5), 2975-2997. doi:10.5194/acp-22-2975-2022
- 560 Peterson, D. A., Campbell, J. R., Hyer, E. J., Fromm, M. D., Kablick, G. P., Cossuth, J. H., & DeLand, M. T. (2018). Wildfire-driven thunderstorms cause a volcano-like stratospheric injection of smoke. *npj Climate and Atmospheric Science*, 1(1), 30. doi:10.1038/s41612-018-0039-3
- Ploeger, F., Konopka, P., Walker, K., & Riese, M. (2017). Quantifying pollution transport from the Asian monsoon anticyclone into the lower stratosphere. *Atmos. Chem. Phys.*, 17(11), 7055-7066. doi:10.5194/acp-17-7055-2017
- 565 Reifenberg, S. F., Martin, A., Kohl, M., Hamryszczak, Z., Tadic, I., Röder, L., Crowley, D. J., Fischer, H., Kaiser, K., Schneider, J., Dörich, R., Crowley, J. N., Tomsche, L., Marsing, A., Voigt, C., Zahn, A., Pöhlker, C., Holanda, B., Krüger, O. O., Pöschl, U., Pöhlker, M., Jöckel, P., Dorf, M., Schumann, U., Williams, J., Curtius, J., Harder, H., Schlager, H., Lelieveld, J., Pozzer, A. (2021). Impact of reduced emissions on direct and indirect aerosol radiative forcing during COVID-19 lockdown in Europe. *Atmos. Chem. Phys. Discuss.*, 2021, 1-23. doi:10.5194/acp-2021-1005
- 570 Rolph, G., Stein, A., & Stunder, B. (2017). Real-time Environmental Applications and Display sYstem: READY. *Environmental Modelling & Software*, 95, 210-228. doi:<https://doi.org/10.1016/j.envsoft.2017.06.025>
- Schäfer, S., Lawrence, M., Stelzer, H., Born, W., Low, S., Aaheim, A., Adriázola, P., Betz, G., Boucher, O., Carius, A. (2015). The European transdisciplinary assessment of climate engineering (EuTRACE): Removing greenhouse gases from the atmosphere and reflecting sunlight away from Earth.
- 575 Schiller, C. L., Bozem, H., Gurk, C., Parchatka, U., Königstedt, R., Harris, G. W., Lelieveld, J., Fischer, H. (2008). Applications of quantum cascade lasers for sensitive trace gas measurements of CO, CH<sub>4</sub>, N<sub>2</sub>O and HCHO. *Applied Physics B*, 92(3), 419-430. doi:10.1007/s00340-008-3125-0
- Schmale, J., Schneider, J., Jurkat, T., Voigt, C., Kalesse, H., Rautenhaus, M., Lichtenstern, M., Schlager, H., Ancellet, G., Arnold, F., Gerding, M., Mattis, I., Wendisch, M., Borrmann, S. (2010). Aerosol layers from the 2008 eruptions of Mount Okmok and Mount Kasatochi: In situ upper troposphere and lower stratosphere measurements of sulfate and organics over Europe. *Journal of Geophysical Research*, 115. doi:10.1029/2009jd013628
- 580 Schneider, J., Hings, S. S., Hock, N. B., Weimer, S., Borrmann, S., Fiebig, M., Petzold, A., Busen, R., Kärcher, B. (2006). Aircraft-based operation of an aerosol mass spectrometer: Measurements of tropospheric aerosol composition. *Journal of Aerosol Science*, 37(7), 839-857. doi:<https://doi.org/10.1016/j.jaerosci.2005.07.002>
- 585 Schneider, J., Weigel, R., Klimach, T., Dragoneas, A., Appel, O., Hünig, A., Molleker, S., Köllner, F., Clemen, H. C., Eppers, O., Hoppe, P., Hoor, P., Mahnke, C., Krämer, M., Rolf, C., Groöß, J. U., Zahn, A., Obersteiner, F., Ravegnani, F., Ulanovsky, A., Schlager, H., Scheibe, M., Diskin, G. S., DiGangi, J. P., Nowak, J. B., Zöger, M., Borrmann, S. (2021). Aircraft-based observation of meteoric material in lower-stratospheric aerosol particles between 15 and 68°&thinsp;N. *Atmos. Chem. Phys.*, 21(2), 989-1013. doi:10.5194/acp-21-989-2021
- 590 Schulte, P., & Schlager, H. (1996). In-flight measurements of cruise altitude nitric oxide emission indices of commercial jet aircraft. 23(2), 165-168. doi:<https://doi.org/10.1029/95GL03691>
- Schulz, C., Schneider, J., Amorim Holanda, B., Appel, O., Costa, A., de Sá, S. S., Dreiling, V., Fütterer, D., Jurkat-Witschas, T., Klimach, T., Knote, C., Krämer, M., Martin, S. T., Mertes, S., Pöhlker, M. L., Sauer, D., Voigt, C., Walser, A., Weinzierl, B., Ziereis, H., Zöger, M., Andreae, M. O., Artaxo, P., Machado, L. A. T., Pöschl, U., Wendisch, M., Borrmann, S. (2018). Aircraft-based observations of isoprene-epoxydiol-derived secondary organic aerosol (IEPOX-SOA) in the tropical upper troposphere over the Amazon region. *Atmos. Chem. Phys.*, 18(20), 14979-15001. doi:10.5194/acp-18-14979-2018
- Schumann, U., Bugliaro, L., Dörnbrack, A., Baumann, R., Voigt, C. (2021). Aviation Contrail Cirrus and Radiative Forcing Over Europe During 6 Months of COVID-19. 48(8), e2021GL092771. doi:<https://doi.org/10.1029/2021GL092771>
- 600 Schumann, U., Poll, I., Teoh, R., Koelle, R., Spinielli, E., Molloy, J., Koudis, G. S., Baumann, R., Bugliaro, L., Stettler, M., Voigt, C. (2021). Air traffic and contrail changes over Europe during COVID-19: a model study. *Atmos. Chem. Phys.*, 21(10), 7429-7450. doi:10.5194/acp-21-7429-2021
- Seinfeld, J. H., & Pandis, S. N. (2006). *Atmospheric chemistry and physics: from air pollution to climate change*: John Wiley & Sons.



- 605 Sheng, J.-X., Weisenstein, D. K., Luo, B.-P., Rozanov, E., Stenke, A., Anet, J., Bingemer, H., Peter, T. (2015). Global atmospheric sulfur budget under volcanically quiescent conditions: Aerosol-chemistry-climate model predictions and validation. *120*(1), 256-276. doi:<https://doi.org/10.1002/2014JD021985>
- Speidel, M., Nau, R., Arnold, F., Schlager, H., & Stohl, A. (2007). Sulfur dioxide measurements in the lower, middle and upper troposphere: Deployment of an aircraft-based chemical ionization mass spectrometer with permanent in-flight calibration. *Atmospheric Environment*, *41*(11), 2427-2437. doi:10.1016/j.atmosenv.2006.07.047
- 610 Stein, A., Draxler, R., Rolph, G., & Stunder, B. (2015). B., cohen, md, and ngan, f.: NOAA's HYSPLIT atmospheric transport and dispersion modeling system. *Am. Meteorol. Soc.*, *96*, 2059-2077.
- Stockwell, W. R., & Calvert, J. G. (1983). The mechanism of the HO-SO<sub>2</sub> reaction. *Atmospheric Environment (1967)*, *17*(11), 2231-2235. doi:[https://doi.org/10.1016/0004-6981\(83\)90220-2](https://doi.org/10.1016/0004-6981(83)90220-2)
- 615 Tomsche, L., Pozzer, A., Ojha, N., Parchatka, U., Lelieveld, J., & Fischer, H. (2019). Upper tropospheric CH<sub>4</sub> and CO affected by the South Asian summer monsoon during the Oxidation Mechanism Observations mission. *Atmos. Chem. Phys.*, *19*(3), 1915-1939. doi:10.5194/acp-19-1915-2019
- van Heerwaarden, C. C., Mol, W. B., Veerman, M. A., Benedict, I., Heusinkveld, B. G., Knap, W. H., Kazadzis, S., Kouremeti, N., Fiedler, S. (2021). Record high solar irradiance in Western Europe during first COVID-19 lockdown largely due to unusual weather. *Communications Earth & Environment*, *2*(1), 37. doi:10.1038/s43247-021-00110-0
- 620 Vogel, B., Günther, G., Müller, R., Grooß, J.-U., Afchine, A., Bozem, H., Hoor, P., Krämer, M., Müller, S., Riese, M., Rolf, C., Spelten, N., Stiller, G. P., Ungermann, J., Zahn, A. (2016). Long-range transport pathways of tropospheric source gases originating in Asia into the northern lower stratosphere during the Asian monsoon season 2012. *Atmospheric Chemistry and Physics*, *16*(23), 15301-15325. doi:10.5194/acp-16-15301-2016
- 625 Vogel, B., Günther, G., Müller, R., Grooß, J. U., Hoor, P., Krämer, M., Müller, S., Zahn, A., Riese, M. (2014). Fast transport from Southeast Asia boundary layer sources to northern Europe: rapid uplift in typhoons and eastward eddy shedding of the Asian monsoon anticyclone. *Atmospheric Chemistry and Physics*, *14*(23), 12745-12762. doi:10.5194/acp-14-12745-2014
- Vogel, B., Müller, R., Günther, G., Spang, R., Hanumanthu, S., Li, D., Riese, M., Stiller, G. P. (2019). Lagrangian simulations of the transport of young air masses to the top of the Asian monsoon anticyclone and into the tropical pipe. *Atmospheric Chemistry and Physics*, *19*(9), 6007-6034. doi:10.5194/acp-19-6007-2019
- 630 Voigt, C., Jessberger, P., Jurkat, T., Kaufmann, S., Baumann, R., Schlager, H., Bobrowski, N., Giuffrida, G., Salerno, G. (2014). Evolution of CO<sub>2</sub>, SO<sub>2</sub>, HCl, and HNO<sub>3</sub> in the volcanic plumes from Etna. *Geophysical Research Letters*, *41*(6), 2196-2203. doi:10.1002/2013gl058974
- Voigt, C., Lelieveld, J., Schlager, H., Schneider, J., Curtius, J., Meerkötter, R., Sauer, D., Bugliaro, L., Bohn, B., Crowley, J. N., Erbertseder, T., Groß, S., Hahn, V., Li, Q., Mertens, M., Pöhlker, M. L., Pozzer, A., Schumann, U., Tomsche, L., Williams, J., Zahn, A., Andreae, M., Borrmann, S., Bräuer, T., Dörich, R., Dörnbrack, A., Edtbauer, A., Ernle, L., Fischer, H., Giez, A., Granzin, M., Grewe, V., Harder, H., Heinritzi, M., Holanda, B. A., Jöckel, P., Kaiser, K., Krüger, O. O., Lucke, J., Marsing, A., Martin, A., Matthes, S., Pöhlker, C., Pöschl, U., Reifenberg, S., Ringsdorf, A., Scheibe, M., Tadic, I., Zauner-Wieczorek, M., Henke, R., Rapp, M. (2022). Cleaner skies during the COVID-19 lockdown. *Bulletin of the American Meteorological Society*. doi:10.1175/bams-d-21-0012.1
- 635 Voigt, C., Schumann, U., Jurkat, T., Schäuble, D., Schlager, H., Petzold, A., Gayet, J. F., Krämer, M., Schneider, J., Borrmann, S., Schmale, J., Jessberger, P., Hamburger, T., Lichtenstern, M., Scheibe, M., Gourbeyre, C., Meyer, J., Kübbeler, M., Frey, W., Kalesse, H., Butler, T., Lawrence, M. G., Holzäpfel, F., Arnold, F., Wendisch, M., Döpelheuer, A., Gottschaldt, K., Baumann, R., Zöger, M., Sölch, I., Rautenhaus, M., Dörnbrack, A. (2010). In-situ observations of young contrails – overview and selected results from the CONCERT campaign. *Atmos. Chem. Phys.*, *10*(18), 9039-9056. doi:10.5194/acp-10-9039-2010
- 640 von Hobe, M., Ploeger, F., Konopka, P., Kloss, C., Ulanowski, A., Yushkov, V., Ravegnani, F., Volk, C. M., Pan, L. L., Honomichl, S. B., Tilmes, S., Kinnison, D. E., Garcia, R. R., Wright, J. S. (2021). Upward transport into and within the Asian monsoon anticyclone as inferred from StratoClim trace gas observations. *Atmos. Chem. Phys.*, *21*(2), 1267-1285. doi:10.5194/acp-21-1267-2021
- Williamson, C. J., Kupc, A., Rollins, A., Kazil, J., Froyd, K. D., Ray, E. A., Murphy, D. M., Schill, G. P., Peischl, J., Thompson, C., Bourgeois, I., Ryerson, T. B., Diskin, G. S., DiGangi, J. P., Blake, D. R., Bui, T. P. V., Dollner, M., Weinzierl, B., Brock, C. A. (2021). Large hemispheric difference in nucleation mode aerosol concentrations in the lowermost stratosphere at mid- and high latitudes. *Atmos. Chem. Phys.*, *21*(11), 9065-9088. doi:10.5194/acp-21-9065-2021
- 650 Zahn, A., Weppner, J., Widmann, H., Schlote-Holubek, K., Burger, B., Kühner, T., Franke, H. (2012). A fast and precise chemiluminescence ozone detector for eddy flux and airborne application. *Atmos. Meas. Tech.*, *5*(2), 363-375. doi:10.5194/amt-5-363-2012
- Ziereis, H., Schlager, H., Schulte, P., van Velthoven, P. F. J., & Slemr, F. (2000). Distributions of NO, NO<sub>x</sub>, and NO<sub>y</sub> in the upper troposphere and lower stratosphere between 28° and 61°N during POLINAT 2. *105*(D3), 3653-3664. doi:<https://doi.org/10.1029/1999JD900870>
- 655